Modeling, Simulation and Verification of Contactless Power Transfer Systems

J. Serrano[1,*], M. Pérez-Tarragona[1], C. Carretero[2], J. Acero[1].

[1]Department of Electronic Engineering and Communications. Universidad de Zaragoza.
Maria de Luna, 1. 50018 Zaragoza. Spain.
[2]Department of Applied Physics. Universidad de Zaragoza.
Pedro Cerbuna, 12. 50009 Zaragoza, Spain.
[*]E-mail: jserrano@unizar.es

***Abstract*—This work presents the analysis of a wireless power transfer system consisting of two coupled coils and ferrite slabs acting as flux concentrators. The study makes use of Finite Element Method (FEM) simulations to predict the key performance indicators of the system such as coupling, quality factor and winding resistance. The simulations results were compared against experimental measurements on a prototype showing consistence.**

***Keywords*—Wireless power transfer, Electromagnetic modeling, FEM simulation, Inductive Charging.**

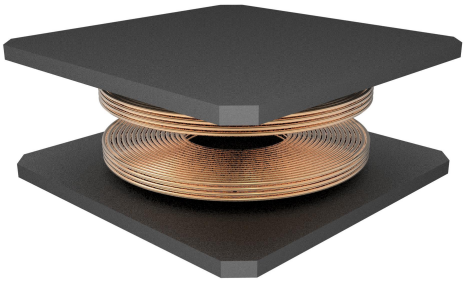

Fig. 1. Wireless power transfer system.

I. Introduction

Wireless power transfer (WPT) applications are taking major importance among market trends thanks to their versatility and user convenience. This solution allows the producers to remove the cables and connectors which are one of the main causes of breakdown. As this technology consolidates, WPT systems are becoming more common and available for a large number of devices. The modeling of these systems is, therefore, of great interest.

Important research efforts were made in the past on the development of this WPT systems [1–4]. The main areas of interest include inductive coupling between the coils [5], power losses in the windings [6–10], and power electronics [11–15]. In terms of the intended application, these systems can be roughly classified in low power magnetic links and high power magnetic links. Low power links are highly limited by size restrictions, i.e. small-sized devices and large separation between coils. These leads to loosely coupled coils and low efficiency in the inductive power transference. On the other hand, high power links are characterized the use of larger coils with higher coupling leading to higher inductive power transference efficiencies [16].

In this work, a simulation model for low power transfer will be presented in order to predict the key performance indicators of the system. These will be later compared against measurements on a prototype.

In order to address this problem, in Section II, key performance indicators will be defined. In Section III, the electromagnetic model will be presented. In Section IV, the simulation procedure with COMSOL will be detailed. In Section V, the model will be experimentally validated by characterizing a prototype. Finally, Section VI gathers the main conclusions of the study.

II. Key performance indicators of low power inductive links

The operating principle of WPT systems is based on Lenz-Faraday's Law, according to which the induced electromotive force in any closed circuit is equal to the negative of the time rate of change of the magnetic flux enclosed by the circuit [17]. An alternating current is driven through the primary coil generating and alternating magnetic field. This field causes a variable flux through the secondary coil, where an electromotive force is induced. The system can be interpreted as a loosy coupled coreless transformer.

The coupling between two coils, k, is defined as usual,

$$k = \frac{M}{\sqrt{L_1 L_2}}, \tag{1}$$

where L_1 is the self-inductance of the primary, L_2 is the self-inductance of the secondary, M is the mutual inductance.

Moreover, the quality factor of a coil is defined as,

$$Q_i = \frac{\omega_0 L_i}{R_i}, \tag{2}$$

where ω_0 is the angular frequency of resonance and $i = 1, 2$ is an index indicating primary or secundary coil.

The efficiency of a WPT for a certain geometry was proven [16] to be a function of the aforementioned variables, being limited by the maximum efficiency [5]:

$$\eta_{max} = \frac{1}{1 + \frac{2}{(kQ)^2}\left(1 + \sqrt{1 + (kQ)^2}\right)} \tag{3}$$

where $Q = \sqrt{Q_1 Q_2}$.

As can be inferred from Equation 3, the efficiency is maximized when the parameter kQ is maximized. Therefore, the parameter kQ will be chosen as a key performance parameter, which introducing Equations 1 and 2, can be expressed as,

$$kQ = \frac{M}{\sqrt{L_1 L_2}} \sqrt{\frac{(\omega_0 L_1)(\omega_0 L_2)}{R_1 R_2}}. \tag{4}$$

The electromagnetic model in the next section will have as main objective to model and correctly predict the variables involved in Equation 4: M, L_1, L_2, R_1 and R_2 which are characteristic of the coils.

III. Electromagnetic Modeling

A. Self and mutual inductance calculation

High frequency devices usually employ multi-stranded litz wire due to its good reduced ac-losses [10]. Litz wire ensures that all the strands in the cable are equivalent among them [8], and therefore the current is equally shared between all of the strands. Under this assumption, the primary inductor can be modeled as a ring-shaped ideal domain with rectangular cross-section through which a constant current density flows. This simplification is graphically represented in Fig. 2, where t_f represents the ferrite's thickness, t_w represents the winding's thickness, r_{ext} and r_{int} are the external and internal radii respectively and indexes 1 and 2 represent primary coil (transmitter) and secondary coil (receiver). Δz is the separation between coils

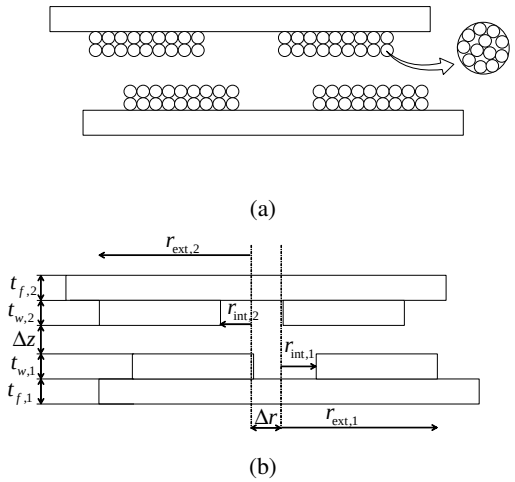

Fig. 2. Cross-section schematic of (a) wireless power transfer system with two coils wound with litz wire and two slabs of ferrite as flux concentrator. (b) Simulation model.

and Δr represents misalignment.

Once the geometry is defined, the current density can be defined as,

$$\vec{\mathbf{J}} = \frac{n \cdot I_0}{t_{w,1}\left(r_{\text{ext},1} - r_{\text{int},1}\right)} \widehat{\varphi} \tag{5}$$

being n the number of turns, I_0 the current and $\widehat{\varphi}$ represents the azimuthal direction of a cylindric coordinate system.

This current generates a magnetic field H and an electric field E, from which the induced electromotive force can be calculated for both coils:

$$V_i = -\oint \vec{\mathbf{E}} \cdot \vec{dl} = -\frac{1}{S_{\text{coil},i}} \int_{V_{\text{coil},i}} E_\varphi dV \tag{6}$$

From were the coil's impedance can be obtained,

$$Z_i = \frac{V_i}{I_0}. \tag{7}$$

The calculation of L_1, L_2 and M is immediate. When coil 1 is excited, L_1 and M are obtained as:

$$L_1 = \frac{\Im\text{m}(Z_1)}{\omega} \tag{8}$$

$$M = \frac{\Im\text{m}(Z_2)}{\omega} \tag{9}$$

When coil 2 is excited, L_2 can be calculated and M can be verified:

$$L_2 = \frac{\Im\text{m}(Z_2)}{\omega} \tag{10}$$

$$M = \frac{\Im\text{m}(Z_1)}{\omega} \tag{11}$$

Note that as the inductors are ideal domains, no power losses take place on them. Therefore, the resulting resistance from $R_i = \Re\mathrm{e}(Z_i)$ would be null. The resistance of the losses are calculated by a separate loss model.

B. Winding resistance calculation

The power losses in the winding can be divided into two groups, depending on their cause. On one hand, dc and skin effect losses produce an associated power loss referred as conduction loss, P_{cond}. On the other hand, induced currents due to proximity effects produce proximity losses, P_{prox}. Both can be modeled by resistances, R_{cond} and R_{prox}, in such a way that $R_i = R_{\mathrm{cond},i} + R_{\mathrm{prox},i}$.

From previous studies [18, 19] the resistance of a circular cross-sectional conductor per unit length (e.g. PCB tracks) is already known:

$$R_{dc,skin,u.l.} = \frac{1}{\pi r_0^2 \sigma} \Phi_{dc,skin}(r_0/\delta) \qquad (12)$$

$$R_{prox,t,u.l.} = \frac{4\pi}{\delta} \Phi_{prox}(r_0/\delta) |H_t|^2 \qquad (13)$$

where r_0 is the strand radius, σ is the conductor electrical conductivity, δ is the skin depth, H_t is the transversal magnetic field and $\Phi_{dc,skin}$ and Φ_{prox} are functions including the geometric and frequency dependences. Their analytical expressions where inferred in [20].

By integrating equations (12) and (13) in inductor domain, and expressing the resistances in terms of cylindrical coordinates (where the index k refers to the coordinates r and z) the conduction resistance $R_{\mathrm{cond},11}$ and proximity resistance $R_{\mathrm{prox},11}$ of one turn made of one strand can be obtained:

$$R_{\mathrm{cond},11} = \frac{l_{av}}{\pi r_0^2 \sigma} \Phi_{dc,skin}(r_0/\delta) \qquad (14)$$

$$R_{\mathrm{prox}\ k,11} = \frac{4\pi}{\sigma} \Phi_{\mathrm{prox}}(r_0/\delta) \left\langle 2\pi r \left| \bar{H}_{0\,i,1} \right|^2 \right\rangle \qquad (15)$$

where $l_{av} = \pi(r_{\mathrm{ext}} + r_{\mathrm{int}})$ represents the average length of the turns, $\bar{H}_{0\,i,1}$ corresponds to the magnetic field generated by the single-wire turn and $\left\langle 2\pi r \left| \bar{H}_{0\,i,1} \right|^2 \right\rangle$ is the averaged square magnetic field in the ideal ring-type inductor volume.

Taking into account that an inductor consist of n turns connected in series, and n_s strands connected in parallel, the relation for conduction losses is straightforward: $R_{\mathrm{cond}} = \frac{n}{n_s} R_{\mathrm{cond},11}$. On the other hand, proximity losses are additive both with turns and strands and proportional to the square of the magnetic field incident on the conductors, $|\bar{H}_0|^2 = n^2 |\bar{H}_{0,1}|^2$. Consequently, $R_{\mathrm{prox}} = n^3 \cdot n_s \cdot R_{\mathrm{prox},11}$.

The resistance of each coil is finally given by

$$R_i = \frac{n}{n_s} R_{\mathrm{cond},11,\mathrm{i}} + n^3 \cdot n_s \cdot R_{\mathrm{prox},11,\mathrm{i}}. \qquad (16)$$

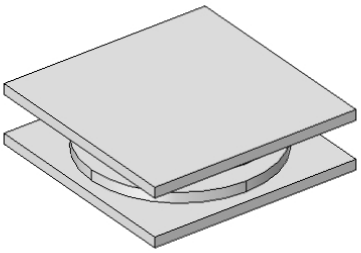

Fig. 3. Model geometry.

TABLE I. System parameters.

Description	Symbol	Value
Nr. Turns	n	20
Nr. Strands	n_s	105
Strand radius	r_s	40 (μm)
Ferrite thickness	t_f	2.5 (mm)
Ferrite side length	l	50 (mm)
Coil external radius	r_{ext}	22 mm
Coil internal radius	r_{int}	10.12 mm
Coil thickness	t_w	2.5 mm
Coil separation	Δz	4 mm
Misalignment	Δr	0-44 mm

IV. Simulation in COMSOL

The model was simulated in COMSOL making use of the AC/DC Module. The geometry is shown in Fig. 3 and the geometric parameters are shown in Table I.

The domains representing the coils are defined as quasi-ideal domains ($\sigma \approx 0$ S/m, $\mu_r = 1$), while the ferrites are characterized by their physical properties ($\sigma \approx 0$ S/m, $\mu_r = 2000$). Firstly, an external current density is set in the primary coil. The current density is calculated according to Equation (5), with a current of $I_0 = 1$ A and the geometric parameters in Table I. The simulations are run in frequency domain, sweeping the frequency from 1 kHz up to 300 kHz. From this simulation the L_1 and M can be calculated. In the second place, the simulation is repeated exciting the secondary coil (receiver) in order to obtain L_2. Moreover, the magnetic field average is obtained in order to calculate the losses according to Equation (15).

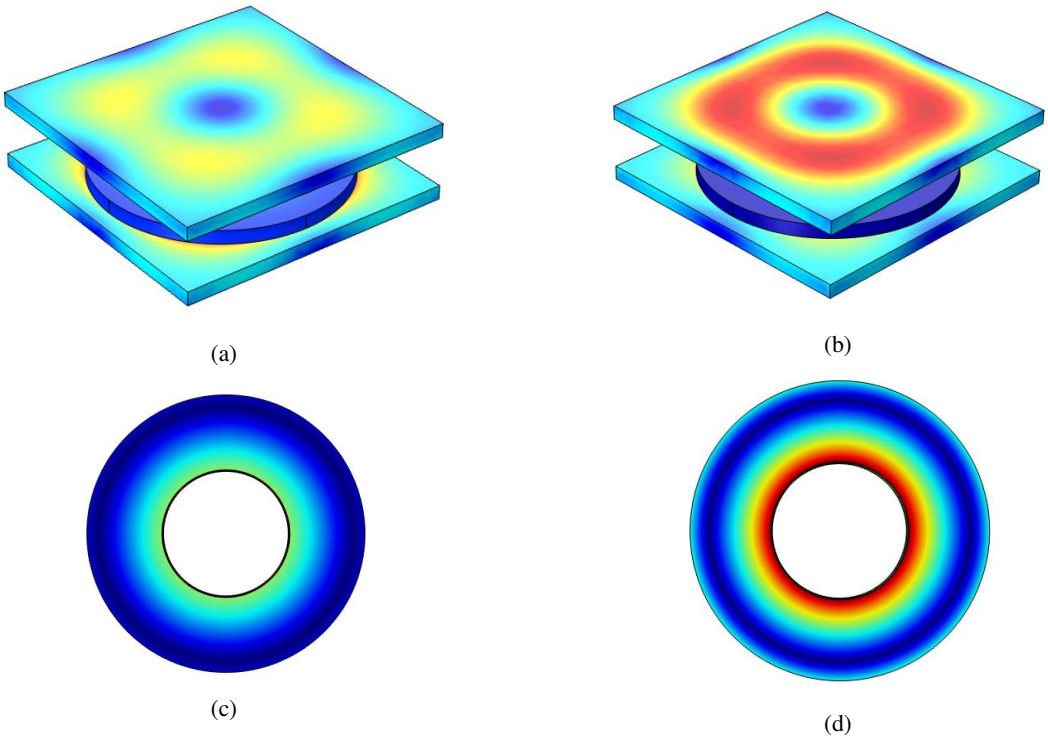

(a) (b) (c) (d)

Fig. 4. Simulation results for the magnetic field $\mathbf{B}$. (a) Complete system. Primary coil is excited, secondary coil is in open circuit. (a) Complete system. Secondary coil is excited, primary coil is in open circuit. (c) Top view of the open-circuited coil. (d) Top view of the excited coil.

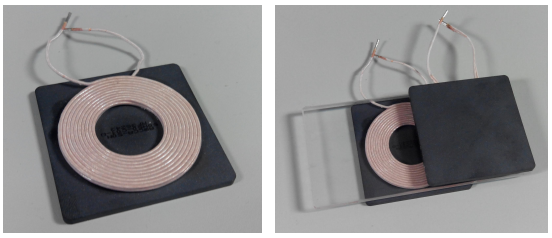

(a) (b)

Fig. 5. Measured prototype. (a) Primary coil (b) Complete system.

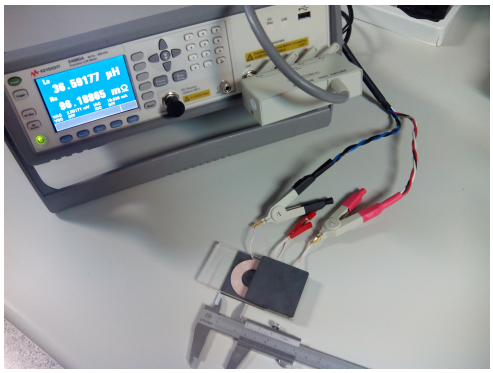

Fig. 6. Measuring setup.

Fig. 5b shows the obtained magnetic field when exciting the primary coil or transmitter and the secondary coil or receiver.

V. Experimental verificaton

In order to verify the model, a prototype was measured with a Keysight E4980A LCR Meter. The system is composed of two coils whose geometric parameters are shown in Table I. Both coils are equal, and therefore their resistance and inductance will be denoted as $R = R_1 = R_2$ and $L = L_1 = L_2$ respectively. The measured prototype is shown in Fig. 5 and the measuring setup is shown in Fig. 6.

The LCR Meter was set to measure series resistance and inductance from 10 kHz to 300 kHz. The results of the self inductances an resistances are compared against the calculations in Fig. 7 for different misalignments. As can be observed, the resistances and and self-inductances slightly decrease with an increasing misalignment. This has low impact in the kQ factor, and therefore in the maximal efficiency. However, the mutual inductance drastically drops when misaligning the coils. Fig. 8 shows a comparison between the calculated value of M and the measured value, which was calculated as a quarter of the difference of the inductance of the series connection of both coils, L_s, and the counter-series connection, L_{cs} [21]:

$$M = \frac{L_s - L_{cs}}{4}. \tag{17}$$

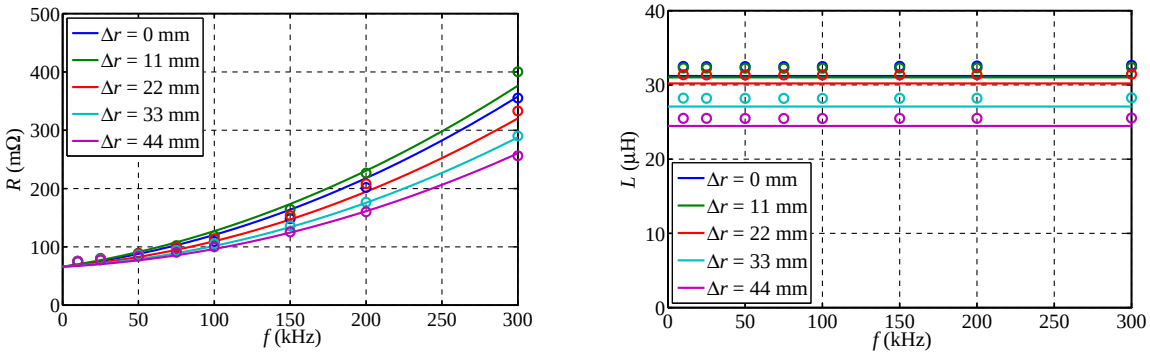

(a) (b)

Fig. 7. Impedance components of the coils as a function of frequency for different misalignments. Simulated impedance components in solid line. Measured impedance components in circles. (a) Resistance. (b) Inductance.

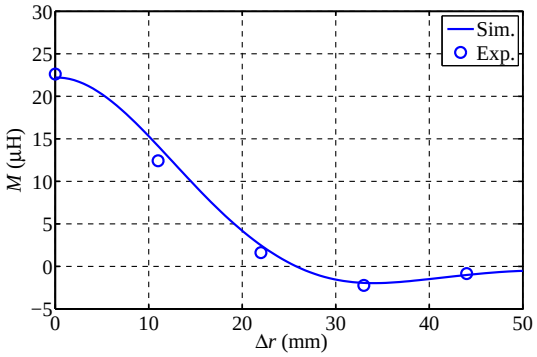

Fig. 8. Mutual inductance as a function of misalignment at 100 kHz. Simulated in solid line. Measured in circles.

In all cases, the simulations are consistent with the experimental characterization.

VI. Conclusions

In this paper, a method for simulating Wireless Power Transfer systems in COMSOL is presented. The method combines analytical developments with Finite Element Method simulations and its main objective is to predict the value of the key performance indicators of Wireless Power Transfer system. In these systems, the maximum efficiency is highly dependent of the product between the coupling factor and the geometric average of the quality factors of both coils. These can be expressed in terms of self-inductances, mutual inductances and resistances. Therefore, the method proposed aims to accurately predict these variables. The simulations were compared against empirical results showing good consistence.

VII. Acknowledgements

This work was partly supported by the Spanish MINECO under Projects TEC2013-42937-R and RTC-2014-1847-6, by the DGA-FSE, and by the BSH Home Appliances Group.

References

[1] C.-G. Kim, D.-H. Seo, J.-S. You, J.-H. Park, and B.-H. Cho, "Design of a contactless battery charger for cellular phone," in *Applied Power Electronics Conference and Exposition, 2000. APEC 2000. Fifteenth Annual IEEE*, vol. 2, pp. 769–773 vol.2, 2000.

[2] B. Choi, J. Nho, H. Cha, T. Ahn, and B. Choi, "Design and implementation of low-profile contactless battery charger using planar printed circuit board windings as energy transfer device," *Industrial Electronics, IEEE Transactions on*, vol. 51, pp. 140–147, Feb 2004.

[3] C.-H. Hu, C.-M. Chen, Y.-S. Shiao, T.-J. Chan, and L.-R. Chen, "Development of a universal contactless charger for handheld devices," in *Industrial Electronics, 2008. ISIE 2008. IEEE International Symposium on*, pp. 99–104, June 2008.

[4] J. Achterberg, E. Lomonova, and J. de Boeij, "Coil array structures compared for contactless battery charging platform," *Magnetics, IEEE Transactions on*, vol. 44, pp. 617–622, May 2008.

[5] R. Bosshard, J. Muhlethaler, J. W. Kolar, and I. Stevanovic, "The pareto front of inductive power transfer coils," in *IECON 2012 - 38th Annual Conference on IEEE Industrial Electronics Society*, pp. 4270–4277, Oct 2012.

[6] J. Ferreira, "Improved analytical modeling of conductive losses in magnetic components," *Power Electronics, IEEE Transactions on*, vol. 9, pp. 127–131, Jan 1994.

[7] J. Ferreira, "Analytical computation of ac resistance of round and rectangular litz wire windings," *Electric Power Applications, IEE Proceedings B*, vol. 139, pp. 21–25, Jan 1992.

[8] C. R. Sullivan and L. W. Losses, "Analytical model for effects of twisting on litz-wire losses," in *2014 IEEE 15th Workshop on Control and Modeling for Power Electronics*

(COMPEL), pp. 1–10, June 2014.

[9] C. R. Sullivan, "Cost-constrained selection of strand diameter and number in a litz-wire transformer winding," in *Industry Applications Conference, 1998. Thirty-Third IAS Annual Meeting. The 1998 IEEE*, vol. 2, pp. 900–906 vol.2, Oct 1998.

[10] C. R. Sullivan, "Optimal choice for number of strands in a litz-wire transformer winding," *IEEE Transactions on Power Electronics*, vol. 14, pp. 283–291, Mar 1999.

[11] F. Forest, S. Faucher, J.-Y. Gaspard, D. Montloup, J.-J. Huselstein, and C. Joubert, "Frequency-synchronized resonant converters for the supply of multiwinding coils in induction cooking appliances," *Industrial Electronics, IEEE Transactions on*, vol. 54, pp. 441–452, Feb 2007.

[12] P. Achara, P. Viriya, and K. Matsuse, "Analysis of a half - bridge inverter for a small-size induction cooker using positive-negative phase-shift control under zvs and non-zvs operation," in *Power Electronics and Drive Systems, 2007. PEDS '07. 7th International Conference on*, pp. 157–163, Nov 2007.

[13] O. Lucía, J. Burdío, I. Millán, J. Acero, and L. Barragán, "Efficiency-oriented design of zvs half-bridge series resonant inverter with variable frequency duty cycle control," *Power Electronics, IEEE Transactions on*, vol. 25, pp. 1671–1674, July 2010.

[14] H. Kotte, R. Ambatipudi, and K. Bertilsson, "High-speed (mhz) series resonant converter (src) using multilayered coreless printed circuit board (pcb) step-down power transformer," *Power Electronics, IEEE Transactions on*, vol. 28, pp. 1253–1264, March 2013.

[15] F. Forest, E. Labouré, F. Costa, and J. Gaspard, "Principle of a multi-load/single converter system for low power induction heating," *Power Electronics, IEEE Transactions on*, vol. 15, pp. 223–230, Mar 2000.

[16] G. Vandevoorde and R. Puers, "Wireless energy transfer for stand-alone systems: a comparison between low and high power applicability," *Sensors and Actuators A: Physical*, vol. 92, no. 1–3, pp. 305 – 311, 2001. Selected Papers for Eurosensors {XIV}.

[17] E. C. E. C. Jordan and K. G. Balmain, *Electromagnetic waves and radiating systems*. Englewood Cliffs, N.J. : Prentice-Hall, 2nd ed ed., 1968.

[18] I. Lope, C. Carretero, J. Acero, R. Alonso, and J. Burdío, "Ac power losses model for planar windings with rectangular cross-sectional conductors," *Power Electronics, IEEE Transactions on*, vol. 29, pp. 23–28, Jan 2014.

[19] I. Lope, C. Carretero, J. Acero, R. Alonso, and J. Burdío, "Frequency-dependent resistance of planar coils in printed circuit board with litz structure," *Magnetics, IEEE Transactions on*, vol. 50, pp. 1–9, Dec 2014.

[20] C. Carretero, J. Acero, and R. Alonso., "TM-TE decomposition of power losses in multi-stranded litz-wires used in electronic devices," *Progress In Electromagnetics Research*, vol. 123, pp. 83–103, December 2012.

[21] C. Carretero, O. Lucia, J. Acero, and J. M. Burdio, "Computational modeling of two partly coupled coils supplied by a double half-bridge resonant inverter for induction heating appliances," *IEEE Transactions on Industrial Electronics*, vol. 60, pp. 3092–3105, Aug 2013.